Effect of Lipid Molecular Structure and Gramicidin A on the Core of Lipid Vesicle Bilayers. A Time-Resolved Fluorescence Depolarization Study†

Johan M. Muller,* Gijsbert van Ginkel, and Ernst E. van Faassen

Department of Molecular Biophysics and Debye Research Institute, Buijs Ballot Laboratory, Utrecht University, Princetonplein 5, 3584 CC Utrecht, The Netherlands

Received June 21, 1995; Revised Manuscript Received October 23, 1995⊗

ABSTRACT: We have investigated the molecular orientational order and reorientational dynamics of the fluorescent probe 1,6-diphenyl-1,3,5-hexatriene (DPH) in the core of the membrane bilayer. Vesicles of lipids of varying unsaturation and headgroup (POPC, DOPC, DLPC, DLLPC, EGGPG, DOPG, DGDG, and SQDG) were studied using the time-resolved fluorescence anisotropy of DPH. Generally, values of the second order parameter $\langle P_2 \rangle$ for DPH are found to be very small. However, this should not be interpreted as DPH having low orientational order as witnessed by large values of the next relevant order parameter $\langle P_4 \rangle$. This implies considerable transverse populations of DPH molecules within the bilayer. In phosphatidylcholines with an acyl chain of 18 carbon atoms, the value of $\langle P_2 \rangle$ for DPH decreases with increasing lipid unsaturation and even attains negative values. No effect of the lipid headgroup on the order and dynamics of DPH is detected. Furthermore, we study the peptide−lipid interaction of the hydrophobic antibiotic gramicidin A (gA) in DOPC vesicles using DPH. The nonchannel conformation has an ordering effect on DPH in the bilayer core, which the channel conformation lacks. This can be understood in terms of the geometrical shape of the gA dimer, as shown previously with the probes TMA-DPH and DPHPC [Muller, J. M., et al. (1995) *Biochemistry 34*, 3092]. We find that for DPH data the conventional Brownian rotational diffusion (BRD) model and the compound motion model (CMM) give equivalent fits. In this respect, DPH differs from TMA-DPH and DPHPC, for which probes only the CMM allowed a consistent interpretation of the molecular orientation.

Biological lipid membranes consist of a mixture of various lipids with differing headgroups and unsaturation of the acyl chains. The physiological properties of these structures have been shown to be linked directly to the composition of this mixture. Therefore, the effects of unsaturation and type of headgroup are crucial to a proper understanding of the relation between lipid composition and membrane function. In addition, membrane proteins are vital to the physiological activity as well as to the structural integrity of biological membranes.

Cell membranes have three main functions; i.e., those of (1) a selectively permeable barrier, (2) a both stable and fluid matrix for reactions of lipophilic substances and active proteins, and (3) a flexible boundary which with the associated proteins can transduce energy and information (Yeagle, 1987). So the membrane must be stable enough to maintain a permeability barrier while being sufficiently fluid to accommodate changes in shape or enclosed volume. In structural terms, a measure of both molecular order and mobility is being called for, e.g., in the electron transport chain and the photosynthetic apparatus, and generally in transport and diffusion within or through the membrane. Biological membranes fulfill these requirements by combining lipids with appropriate physical properties, as, e.g., in plant lipid temperature adaptation. Enzymatic and other peptide activities are affected by the phase and composition of the surrounding lipids as well as the rate of lateral diffusion these lipids allow. As the apolar core of the lipid bilayer is intimately involved in these processes, it is of vital importance to the functions of the membrane.

These observations provided the motivation for extensive research into the structure of model membranes either of a single lipid or of a well-defined simplified lipid composition (Houslay & Stanley, 1983; Cevc & Marsh, 1987; Kotyk et al., 1988). Many studies have concentrated on phosphatidylcholine (PC)[1] lipids. It has been clearly established that introduction of cis-double bonds into the acyl chains of PC lipids causes a more disordered conformation of the hydrocarbon chains in the liquid-crystalline phase (Seelig & Seelig, 1977; Seelig & Waespe-Sarcevic, 1978; Stubbs et al., 1981; Deinum et al., 1988; Korstanje et al., 1989a,b; van Langen et al., 1989). At the same time, the location of this double bond within the acyl chain was found to affect the phase transition temperature of the lipid. The type of headgroup may affect the phase transition temperature, lateral diffusion,

† This work was supported by a research grant to J.M.M. from the Stichting voor Biofysica (Foundation for Biophysics) under the auspices of NWO (Netherlands Organization for Scientific Research).

* Corresponding author.

⊗ Abstract published in *Advance ACS Abstracts,* December 15, 1995.

[1] Abbreviations: AFD, angle-resolved fluorescence depolarization; BRD, Brownian rotational diffusion; CD, circular dichroism; CMM, compound motion model; DGDG, digalactosyldiacylglycerol; DLPC, dilineoylphosphatidylcholine; DLLPC, dilinolenoylphosphatidylcholine; DOPC, dioleoylphosphatidylcholine; DOPG, dioleoylphosphatidylglycerol; DPH, diphenylhexatriene; DPHPC, [(diphenylhexatrienyl)-propanoyl]palmitoylphosphatidylcholine; EGGPC, egg yolk phosphatidylcholine; EPR, electron paramagnetic resonance; ETOH, ethanol; gA, gramicidin A; HPLC, high-performance liquid chromatography; HPTLC, high-performance thin-layer liquid chromatography; NMR, nuclear magnetic resonance spectroscopy; PC, phosphatidylcholine; PG, phosphatidylglycerol; POPC, palmitoyloleoylphosphatidylcholine; SCIC, strong collision in cone; SQDG, sulfoquinovosyldiacylglycerol; SUV, small unilamellar vesicle(s); TFE, 2,2,2-trifluoroethanol; TMA-DPH, (trimethylammonio)diphenylhexatriene.

0006-2960/96/0435-488$12.00/0

lipid order, and acyl chain rotational dynamics (Berde et al., 1980; Kotyk et al., 1988). In this paper, we study how the molecular order and dynamics in the bilayer core are influenced by the degree of acyl chain unsaturation, the type of lipid headgroup, and the presence of a transmembrane peptide.

These problems can be addressed by time-resolved fluorescence anisotropy experiments on probe molecules embedded in lipid vesicle model systems. This technique provides information on the structural order of the lipid membranes and rotational dynamics of the probes on nanosecond time scales set by the fluorescence decay time (Stubbs et al., 1981; Zannoni et al., 1983; Best et al., 1987; van Langen et al., 1987a,b, 1989; Heřman et al., 1994). The fluorescence method requires optically clear samples, but affords much higher sensitivity than, e.g., NMR. Previously, we applied the fluorescent probes TMA-DPH and DPHPC to study the effect of lipid headgroup and unsaturation on the microscopic order and dynamic parameters in the upper regions of the lipid bilayer (Muller et al., 1994a,b). The hydrocarbon core, however, cannot be monitored by the polar probes TMA-DPH and DPHPC. Therefore, in this paper we employ the apolar probe DPH, which is known to reside deep in the hydrocarbon core of the lipid membrane (Davenport et al., 1985; Mulders et al., 1986). We have embedded DPH in a variety of vesicle model membranes of pure lipid composition. This variety was selected to contain a number of lipids with two types of headgroup, i.e., PC and PG, and several degrees of unsaturation in the acyl chains.

Closely related is the problem of the effect of membrane intrinsic peptides on the structure of the lipid bilayer. Many previous investigations have focused on transmembrane and channel-forming peptides, such as gramicidin A (gA), which has become a prototype for studies of protein−lipid systems. Recent reviews are Wallace (1990), Andersen et al. (1992), and Killian (1992). The primary sequence of gA is formyl-L-Val_1-Gly_2-L-Ala_3-D-Leu_4-L-Ala_5-D-Val_6-L-Val_7-D-Val_8-L-Trp_9-D-Leu_{10}-L-Trp_{11}-D-Leu_{12}-L-Trp_{13}-D-Leu_{14}-L-Trp_{15}-ethanolamine. Four important structural aspects of gA have been identified: first, gA can form transmembrane conducting channels. Second, its conformation in the membrane is not unique. A variety of conformations have been identified and may be loosely classified into channel or nonchannel conformations. Third, in high concentrations it can promote the inverted hexagonal H_{II} lipid phase. Fourth, in DOPC the effect of gA on membrane structure has been seen to vary with the depth in the bilayer (Muller et al., 1995). These results are extended here by using DPH to monitor the effects of gA on the hydrocarbon core of DOPC vesicle bilayers.

The aim of this paper is 4-fold. In the first place, we study the effects of lipid unsaturation and headgroup on the ordering and motion of the acyl chains in the inner core of the bilayer. We consider lipids with a phosphatidylcholine headgroup (POPC, EGGPC, DOPC, DLPC, and DLLPC) and with a phosphatidylglycerol headgroup (DOPG and EGGPG). Furthermore, the lipids SQDG and DGDG are investigated because of their importance to plant thylakoid membranes where they form the supporting matrix for light-harvesting complexes. SQDG and DGDG contain 40 and 80%, respectively, of 18:3 polyunsaturated acyl chains (Webb & Green, 1991).

Second, DPH results are correlated with previous findings for the DPH analogue probes TMA-DPH and DPHPC in the same vesicle systems. As each of these probes resides at a different depth in the lipid bilayer, the depth profile of the order and dynamic properties within the bilayer can be sketched by combining results from the three probes.

Third, we study the peptide−lipid interaction of the small hydrophobic antibiotic gramicidin A on DOPC bilayers. In particular, we consider the effect of various concentrations and the two main conformations of gA.

Finally, we address a problem concerning the method of analysis of the fluorescence anisotropy data. For polar fluorescent probes, such as TMA-DPH and DPHPC, the so-called compound motion model (CMM) was shown to afford an improved analysis over conventional models (van der Sijs et al., 1993; Muller et al., 1994a,b). To test this model for DPH itself, we here analyze our data for the systems discussed above with both the CMM and a conventional Brownian rotational diffusion (BRD) model. We note that for vesicles it is essential that the fluorescence anisotropy experiments are time-resolved, as steady-state results cannot disentangle the intertwined effects of orientational order and reorientational dynamics of the probe.

Our main results are the following. The value for the second order parameter $\langle P_2 \rangle$ of DPH is close to 0.0. For PC lipids, it decreases systematically with increasing unsaturation for PC lipids and may even become negative. The choice of headgroup or even its electrical charge does not seriously affect the bilayer core. Correlating our data with previous results on TMA-DPH and DPHPC shows that the ordering of the probes decreases systematically with their depth in the bilayer. The effects of gramicidin A on the hydrocarbon core of DOPC SUV membranes are shown to depend on the concentration and conformation of the peptide. These results agree well with previous findings for the DPHPC and TMA-DPH probes (Muller et al., 1995; Cox et al., 1992). Finally, we found that the CMM gives a good description of the experimental data for a symmetrical probe like DPH. However, the quality of the fits turns out to be equivalent to that obtained with the conventional BRD model. Apart from minor differences in the interpretation of the physical parameters, both models lead to the same conclusions. In this respect, the apolar probe DPH behaves differently from the polar probes TMA-DPH and DPHPC (Muller et al., 1994a,b, 1995). For these, the CMM improved the quality of the fits and was necessary for a consistent interpretation of the molecular orientation of the probes.

MATERIALS AND METHODS

Materials. The phospholipids palmitoyl-Δ^9-oleoyl(16:0,-18:1)phosphatidylcholine (POPC) and Δ^9-dioleoyl(18:1,18:1)phosphatidylcholine (DOPC), egg yolk phosphatidylcholine lipids EGGPC and Δ^9-dioleoyl(18:1,18:1)phosphatidylglycerol (DOPG), and egg phosphatidylglycerolipid EGGPG were obtained from Sigma Chemical Company (St. Louis, MO) and were randomly checked for purity with HPTLC (high-performance thin-layer chromatography). $\Delta^{9,12,15}$-Dilinolenoyl(18:3,18:3)phosphatidylcholine (DLLPC) was purchased from Avanti Polar Lipids and was checked with TLC (thin-layer chromatography). $\Delta^{9,12}$-Dilineoyl(18:2,18:2)phosphatidylcholine (DLPC), the sulfolipid sulfoquinovosyldiacylglycerol (SQDG), and digalactosyldiacylglycerol (DGDG) were purchased from Lipid Products (Surrey, U.K.). SQDG and DGDG were extracted from green plant and were

prior to use tested for purity and oxidation (Koole et al., 1984). The fluorescent probe DPH (1,6-diphenyl-1,3,5-hexatriene) was bought from Molecular Probes Inc. (Junction City, OR) and was dissolved in ethanol to prepare stock solutions which were kept in the dark at 4 °C. Gramicidin A was purified by the Centre for Biomembranes and Lipid Enzymology (CBLE), Utrecht University, The Netherlands, using high-performance liquid chromatography (HPLC) and was a generous gift from Drs. J. A. Killian and H. Tournois. All chemicals used were of analytical grade.

Vesicle Preparation. Small unilamellar vesicles (SUV) of a single lipid were prepared by first dissolving the lipids in chloroform under a nitrogen atmosphere. The appropriate amounts from fresh stock solutions of fluorescent DPH in ethanol were codissolved in order to get a probe to lipid molecular ratio of 1:250. The solvent was removed by flow of nitrogen gas and subsequent storage under high vacuum for 4−6 h. The lipid−probe mixture was hydrated by the addition of 6 mL of 20 mM Tris buffer, pH 8.0, containing 7.5 μM EDTA, and the samples were vigorously vortexed and—with the exception of the DLLPC/DPH system—subsequently sonicated in a bath-type sonicator for 15−45 min until a clear suspension resulted. This suspension was then centrifuged at 100000*g* for 1 h in a Beckman L2-65B ultracentrifuge, and the supernatant was used for experiments. As sonication of DLLPC dispersions led to oxidation of this polyunsaturated lipid, we prepared DLLPC/DPH SUV by extrusion to avoid this oxidation. The cloudy lipid/buffer suspension was extruded subsequently through three Millipore plastic filters with pores of 600, 200, and 100 nm diameter, respectively, using pressurized nitrogen (Mayer et al., 1986). It was checked that both methods of preparation yielded the same results using the data analysis methods described below.

As the effects of gA are expected to be strongest in DOPC (van Echteld et al., 1982; Killian et al., 1987), we selected this lipid to compare the effects of the channel and nonchannel conformations of gA. This peptide was forced to assume these conformations in the DOPC bilayer by codissolving it from a 1 mM solution in trifluoroethanol or ethanol, respectively (Tournois et al., 1987; Killian & Urry, 1988). Before gA was added to the lipid, all traces of the lipid solvents were removed by prior overnight evaporation under high vacuum. Vesicles were prepared by sonication as described above and by subsequent centrifugation at 50000*g* for 1 h in a Sorvall RC5 centrifuge. The conformations of the incorporated gA were confirmed by circular dichroism (CD) measurements on a Jasco J-600 spectrometer (Vogt et al., 1991) as shown previously (Muller et al., 1995). The vesicle size of a number of samples was measured using dynamic light scattering (Ruf et al., 1989) with a Malvern 4700 system equipped with a 25 mW He−Ne laser and Automeasure software version 3.2; we found average diameters of 110 ± 4 and 185 ± 3 nm for vesicles prepared either by sonication and subsequent centrifugation or by extrusion, respectively, as described above.

All clear vesicle suspensions were kept in the dark, under a nitrogen atmosphere and at low temperatures as much as possible, and were used for measurements within 3 days after preparation. Blank vesicle suspensions without DPH were also prepared for the measurement of elastic light scattering. The lipid concentrations in the samples were obtained from phosphorus determinations (Chen et al., 1956) on the phospholipids, galactose determinations on DGDG (Dubois et al., 1956), and sulfate determination on SQDG (Spencer, 1960).

Time-Resolved Fluorescence Anisotropy and Lifetime Measurements. The time-resolved measurements were performed with the Synchrotron Radiation Source (SRS) in Daresbury (U.K.) operating in single-bunch mode at a 3 MHz repetition rate with a 250 ps pulse width. The excitation wavelength for DPH was set with a SPEX monochromator at 360 ± 3 nm, well away from the excitation bands of the intrinsic tryptophan fluorescence of gramicidin. The emission fluorescence wavelength was defined using a 438 ± 7 nm Balzers interference filter and a Schott GG395 cutoff filter. The standard electronic setup for time-correlated single photon counting as described previously (van Langen et al., 1989) was used. The photomultiplier tube (PMT, Philips XP2020Q) was Peltier-cooled down to −20 °C and fed with −2700 V. The correction *G*-factor for the differential sensitivity to the polarized fluorescence light of the PMT and optics was found to be 1.000 ± 0.005 during the experiments. All experiments were done at the ambient room temperature of 20 ± 2 °C. To record complete decay curves within the range of 1022 channels of the multichannel analyzer (MCA), the channel width of 0.080 ns was used; the elapsed real and live times of the measurement were stored in channels 1023 and 1024 of the MCA. The excitation flash profile was obtained from the elastic scattering of the blank vesicle sample monitored at 438 nm. In the anisotropy experiments, the parallel and perpendicular components of the emitted fluorescence light were collected in an alternating sequence for 25 s each. The count rate was kept at less than 1% of the synchrotron repetition rate of 3 MHz to avoid photon pulse pile-up in the electronics. The intensity of elastically scattered light from the blank vesicle samples was found to be less than 1% of that in the maximum of the fluorescent signal. Apart from the fluorescence anisotropy measurements, separate lifetime data were obtained for each vesicle sample by setting the emission polarizer under the magic angle of 54.7° with the vertical polarization direction.

Brownian Rotational Diffusion and Compound Motion Model for the Time-Resolved Fluorescence Anisotropy. In the time-resolved fluorescence anisotropy experiments described here, a sample of lipid vesicles doped with DPH in aqueous suspension was illuminated by a flash of vertically polarized light to excite the probe; subsequently, the decay of the fluorescence emission was monitored in both vertically (||) and horizontally (⊥) polarized light. The time-dependent intensities of these components can be expressed (Lakowicz, 1986) in terms of the anisotropy decay $r(t)$ and the intrinsic fluorescence decay function $D(t)$ of the probe molecule as

$$I_{||}(t) = (1/3)D(t)[1 + 2r(t)] \quad (1)$$

$$I_{\perp}(t) = (1/3)D(t)[1 - r(t)]$$

The anisotropy decay is governed by the dynamic behavior of the transition dipoles of the probe molecules in the vesicle membrane. We make the usual assumption (Best et al., 1987; van Langen et al., 1987a,b; van Gurp et al., 1988; Muller et al., 1994a,b) that DPH in both its ground and its

excited electronic states is an effectively cylindrically symmetric molecule. Furthermore, we assume that its absorption transition dipole moment lies along its long molecular symmetry axis, and write the anisotropy as a sum of three correlation functions, $G_k(t)$, $k = 0, 1, 2$:

$$r(t) = r(t=0)[G_0(t) + 2G_1(t) + 2G_2(t)] \quad (2a)$$

The initial and final anisotropies are of special relevance as they are directly related to structural parameters of the probe and the membrane. They are independent of the model chosen for the probe molecular motion, i.e.

$$r(t=0) = 0.4P_2[\cos(\beta_\nu)] \quad (2b)$$

and

$$r(t=\infty) = r(t=0)\langle P_2\rangle^2 \quad (2c)$$

where P_2 is the second Legendre polynomial, β_ν is the angle between the emission dipole and the long molecular symmetry axis of DPH, and $\langle P_2\rangle_{BF}$ is the second order parameter for the fluorophore in the bilayer. In this paper, we treat β_ν as a free parameter during the fit; this choice deserves some comment as it differs from fitting procedures of other groups (e.g., Straume & Litman, 1987a,b), where β_ν is kept at a fixed value. We prefer to keep β_ν as a free floating parameter for four reasons: (1) the fixing of β_ν leads to an unphysical restriction of the initial anisotropy decay and so of the diffusional parameter $D_\perp$; (2) the energy levels of DPH are sensitive to its environment (Itoh & Kohler, 1987); this should be reflected in changes of the wavefunctions and transition moments as well; (3) β_ν may depend on the lipid hydration as shown by experiments on EGGPC (van Langen et al., 1987a); and (4) β_ν is affected by the surrounding matrix as shown by the fact that $\beta_\nu = 15°$ in a matrix of unstretched PMMA [poly(methyl methacrylate)] (van Gurp et al., 1989); this value is much smaller than that found in lipid bilayers.

The orientational correlation functions $G_k(t)$ may be calculated from the model used to describe the thermally induced reorientation of the probe. In this paper, we consider two models, i.e., the conventional Brownian rotational diffusion (BRD) model and the so-called compound motion model (CMM). In the BRD model, the probe molecule undergoes small-step angular diffusion in an angle-dependent ordering quasi-potential; this potential mimicks the influence of the lipid environment (Zannoni et al., 1983; van Langen et al., 1989). The CMM is an extension of the BRD model: it assumes that the probes have an additional degree of freedom. They are supposed to experience rapid, though restricted, movements within a fluctuating free volume in the lipid bilayer which is modeled as a slowly rotating cage or cone (van der Sijs et al., 1993). As these movements can be described by strong collision dynamics, this rattling motion was dubbed strong collision in cone (SCIC). The CMM was shown to afford an improved interpretation of fluorescence anisotropy data for the polar probes TMA-DPH and DPHPC in lipid bilayers (Muller et al., 1994a,b, 1995). We shall test the two models by analyzing the data for DPH with each of them.

So far, the CMM has only been applied to TMA-DPH and DPHPC, and we will now extend it to DPH. Due to its apolarity, DPH resides within the hydrocarbon core of the lipid bilayer. As before, we assume that the orientational distribution function, $f(\beta_{BC})$, of the CMM cones depends exclusively on the angle β_{BC} between the cone director (C) and the bilayer normal (B). As the two terminal phenyl rings of DPH are indistinguishable, this probe possesses a plane of symmetry through its center. Therefore, $f(\beta_{BC})$ should be an even function of $\cos(\beta_{BC})$. A suitable parametrization is chosen as

$$f(\beta_{BC}) = N \exp\{-\lambda_2 P_2[\cos(\beta_{BC})] - \lambda_4 P_4[\cos(\beta_{BC})]\} \quad (3)$$

where N normalizes the distribution. The corresponding order parameters for the cone director are then given by the following averages over the Legendre polynomials P_L:

$$\langle P_L\rangle_{BC} = \int d\beta_{BC} \sin(\beta_{BC}) P_L[\cos(\beta_{BC})] f(\beta_{BC}),\ L = 0, 1, 2, \ldots \quad (4a)$$

For an even distribution function as given in eq 3, the odd order parameters, e.g. $\langle P_1\rangle_{BC}$ and $\langle P_3\rangle_{BC}$, vanish. Similarly, we define the order parameters of the fluorophore (F) with respect to the local bilayer normal (B) as

$$\langle P_L\rangle_{BF} = \int d\beta_{BF} \sin(\beta_{BF}) P_L[\cos(\beta_{BF})] F(\beta_{BF}),\ L = 0, 1, 2, \ldots \quad (4b)$$

where $F(\beta_{BF})$ is the orientational distribution function of the fluorophore in the bilayer.

Following the prescription of the CMM, the orientational order of the DPH molecule is determined by two ingredients: (1) the order of the cones with respect to the bilayer (BC); (2) the order of the fluorophore within a cone (CF). Therefore, the order parameters $\langle P_L\rangle_{BF}$ of the DPH fluorophores with respect to the bilayer take the form:

$$\langle P_L\rangle_{BF} = \langle P_L\rangle_{BC}\langle P_L\rangle_{CF} \quad (5)$$

with $L = 1, 2, \ldots$ The $\langle P_L\rangle_{CF}$ values are calculated using the standard expressions for the wobble-in-cone model as given in the appendix of Muller et al. (1994a). Using the $\langle P_L\rangle_{BF}$ order parameters, the distribution function $F(\beta_{BF})$ of the probe in the bilayer according to the CMM can be reconstructed using the relation

$$F(\beta_{BF}) = \sum P_L[\cos(\beta_{BF})]\langle P_L\rangle_{BF},\ L = 0, 1, 2, \ldots \quad (6)$$

In principle, the compound motion model contains four independent dynamic parameters, i.e., $D_{||}$, $D_\perp$, $d_{||}$, and $d_\perp$. The index || denotes the motion around the director while $\perp$ stands for the reorientation of the director itself. The diffusion constants $d_{||}$ and $d_\perp$ characterize the fast in-cone motion. However, $d_{||}$ does not affect the anisotropy decay of DPH as the absorption moment dipole lies along the long molecular symmetry axis of the probe. $d_\perp$ accounts for the much faster motion of DPH within the cone and is related to the rotational correlation time as $\tau_{SC} = 1/d_\perp$. The diffusion constants $D_{||}$ and $D_\perp$ describe the cone rotation around its director and the motion of this director itself, respectively. For reasons given previously (Muller et al., 1994a), we fix $D_{||}$ to $D_{||} = 5D_\perp$.

Numerical Methods. The numerical analysis of the time-resolved experimental data was carried out using the ZXSSQ FORTRAN routine from the IMSL program library to fit the data to the model with the nonlinear least-squares method of Levenberg and Marquardt. The experimental decay curves

from the time-resolved experiment were analyzed using a reiterative nonlinear least-squares deconvolution technique (Cundall & Dale, 1983). The consistency of the resulting parameter set was checked in two ways. First, by integrating the time-resolved fluorescence intensity decays, we compute the value for the steady-state anisotropy r_{ss} from the standard expression

$$r_{ss} = (i_{||} - i_{\perp})/(i_{||} + 2i_{\perp})$$

Here $i_{||}$ and $i_{\perp}$ denote the integrated intensities of $I_{||}(t)$ and $I_{\perp}(t)$, respectively. For a number of samples, the r_{ss} was independently measured in a steady-state experiment using a SPF 500 SLM-Aminco spectrofluorometer equipped with polarizers. In all cases considered, full agreement within experimental error was found. The second control experiment entailed separate measurement of the intrinsic fluorescence decay function $D(t)$. This function was well represented by the biexponential

$$D(t) = \alpha_1 \exp(-t/\tau_1) + \alpha_2 \exp(-t/\tau_2)$$

This function was compared with the intrinsic decay function found from the analysis of the time-resolved anisotropy data. Again, full agreement was found in all cases considered. In the literature, fluorescence decays are often characterized by a mean fluorescence lifetime defined as

$$\langle\tau_F\rangle = \sum_{i=1,2} \alpha_i\tau_i^2 / \sum_{i=1,2} \alpha_i\tau_i$$

In the anisotropy model fit using the CMM, the following 11 free parameters were optimized: (1−2) the fluorescence decay amplitudes α_1 and α_2; (3−4) the fluorescence decay lifetime components τ_1 and τ_2; (5) the factor $P_2[\cos(\beta_\nu)]$, where β_ν is the emission dipole angle in the molecular frame; (6−7) the BRD potential parameters λ_2 and λ_4; (8) the slow rotational diffusion coefficient $D_\perp$ for the motion of the cone containing the probe; (9) the SCIC cone angle θ_{cone}; (10) the SCIC fast diffusion coefficient $d_\perp$ of the probe within the cone; and (11) a parameter to account for a time shift between the excitation profile and both fluorescence emission signals. The BRD model fit lacks cone parameters 9 and 10.

RESULTS AND DISCUSSION

We investigated the orientational order and reorientational dynamics of DPH in the core of the lipid bilayer. For the analysis of the anisotropy data, two models were used, namely, the BRD model and the recent compound motion model (CMM). We will first discuss the model aspects of the results.

Comparison of BRD and CMM Results. The CMM distinguishes itself from the BRD model by its inclusion of a rattling motion for the probe in a cone within the lipid bilayer; this cone represents a fluctuating pocket or void between adjacent lipid acyl chains. We here compare results obtained separately with each model, which are collected in the Table pairs 2A,B and 4A,B.

Four systematic similarities and discrepancies between the BRD and CMM analyses may be identified. In the first place, the CMM does not reduce the values of $\chi^2_{reduced}$ for the fits significantly and only marginally improves the quality of the fits with respect to the BRD model (residue and residue autocorrelation plots not shown). Therefore, the CMM parameters characterizing the internal cone motion can only be determined with low precision. In the second place, CMM consistently predicts smaller values for β_ν than does BRD. This is expected as the cone angle θ_{cone} also contributes to the initial drop of the anisotropy $r(t=0)$ [for a detailed discussion, we refer to section 4 in Muller et al. (1994a)]. Thirdly, the distribution functions for DPH in DOPC vesicles in Figure 1 show that although the CMM gives fewer molecules oriented perpendicular to the bilayer normal, both models predict a sizable transverse population. In this respect, DPH behaves very differently from its polar analogues TMA-DPH and DPHPC; for those probes, the CMM practically eliminated any transverse population. In the fourth place, the molecular motion is parameterized by the CMM with two parameters, whereas this motion in the BRD approach is represented by a single parameter, $D_\perp$. Therefore, CMM leads to consistently smaller values of $D_\perp$ than BRD.

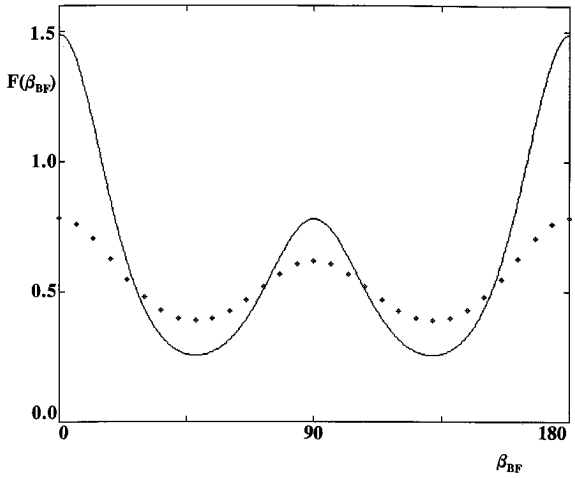

FIGURE 1: Orientational distribution functions $F(\beta_{BF})$ for DPH embedded in small unilamellar vesicle systems of DOPC found using the BRD (solid curve) and CMM (diamonds) models, respectively. β_{BF} is the angle (degrees) of the long molecular axis of the probe with respect to the bilayer normal. The temperature was 20 °C. Both models predict sizable populations of DPH perpendicular to the bilayer normal.

Apart from these differences in details, we note that the CMM and BRD models lead to comparable results. In particular, both predict a sizable population of probes oriented perpendicular to the membrane. However, we stress that the physical content of the models is very different. The lack of discrimination between the two models derives directly from the choice of the fluorescence anisotropy $r(t)$ as the physical observable. As shown in eq 2, this observable appears as the sum over three separate correlation functions $G_0(t)$, $G_1(t)$, and $G_2(t)$. Our simulations show that these individual correlation functions do discriminate well between the two models although both lead to identical predictions for the total sum $r(t)$. This is exemplified in Figure 2 for DPH in EGGPG vesicles. We note that these correlation functions are experimentally accessible in principle: they may be extracted from angle-resolved as well as time-resolved fluorescence depolarization experiments on oriented planar lipid samples (van Langen et al., 1988; van der Heide et al., 1993). We have plotted the predictions of the BRD and CMM models for the correlation functions of DPH in EGGPG vesicles. While the sum of the correlation functions

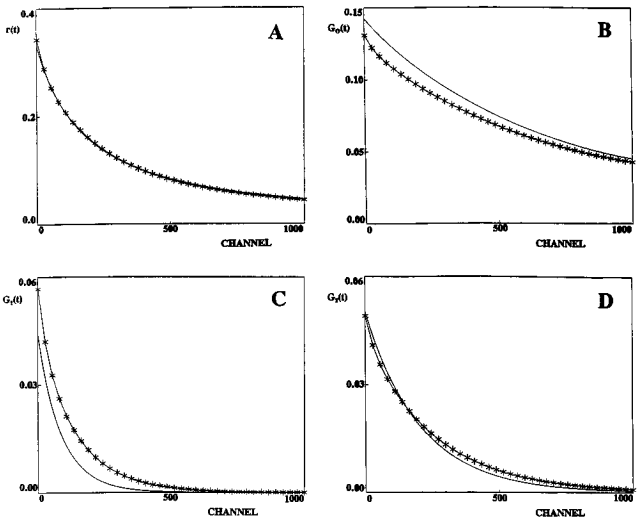

FIGURE 2: Numerical results from the BRD (solid line) and CMM (string of asterisks) models. Parameters are taken from Table 2A,B and represent DPH in EGGPG SUV. The channel width is 10 ps. Figure 2A shows the simulated time-resolved fluorescence anisotropy decay $r(t)$ of DPH resulting from an ideal $\delta(t)$ light pulse. Here both models are indistinguishable. Panels B, C, and D give predictions for the separate contributions of the underlying correlation functions $G_0(t)$, $G_1(t)$ and $G_2(t)$, respectively. Here clear discrepancies emerge for $G_0(t)$ and $G_1(t)$.

Table 1: Effect of Lipid Structure on the Steady-State Anisotropy and Fluorescence Lifetimes of DPH in Small Unilamellar Vesicles[a]

lipid	r_{ss}	α_1	τ_1 (ns)	α_2	τ_2 (ns)	$\langle\tau\rangle_F$ (ns)
POPC	0.077	0.14	3.4	0.86	8.9	8.6
DOPC	0.060	0.15	3.3	0.85	8.2	7.9
DLPC	0.048	0.18	3.3	0.82	8.0	7.6
DLLPC	0.067	0.22	2.6	0.78	8.0	7.6
EGGPG	0.098	0.15	3.9	0.85	9.3	8.9
DOPG	0.065	0.21	5.2	0.79	9.0	8.5
SQDG	0.042	0.77	6.6	0.23	12.2	8.6
DGDG	0.069	0.21	4.3	0.79	8.6	8.1

[a] Both the results for the phosphatidylcholine and phosphatidylglycerol lipids are given in the order of increasing unsaturation. The temperature was 20 °C. The estimated uncertainties are as follows: r_{ss}, 0.003; lifetime parameters α_1, τ_1, α_2, τ_2, and $\langle\tau_F\rangle$, 5%. Values for r_{ss} are seen to be low for all lipids studied, with no clear correlation to lipid unsaturation. The mean fluorescence lifetime $\langle\tau_F\rangle$, however, decreases with unsaturation.

is practically the same with each model, as reflected by the equivalent fits for $r(t)$ discussed above, clear discrepancies emerge for $G_0(t)$ and $G_1(t)$. This implies that time- and angle-resolved experiments can discriminate between both models. We will now consider in detail the experimental results for vesicles of various pure lipids and for DOPC vesicles containing gramicidin A.

Vesicles of PC Lipids with Increasing Unsaturation, PG Lipids, and the Plant Lipids SQDG and DGDG. Table 1 gives results for the steady-state anisotropy r_{ss} and the fluorescence lifetime components for DPH. r_{ss} is easily experimentally accessible and is often taken as a measure of so-called membrane fluidity. However, an increase of r_{ss} may be explained by any or a combination of the following mechanisms: (a) higher molecular order; (b) slower rotational diffusion; or (c) decrease of the fluorescence lifetimes. These mechanisms can only be disentangled by time-resolved anisotropy measurements. From Table 1, no clear correlation between r_{ss} and the unsaturation of the lipids emerges. The values for r_{ss} turn out to be quite low in all systems, i.e., less than 0.10. The mean fluorescence lifetime is seen to decrease with unsaturation. This agrees with previous observations for TMA-DPH in SUV (van Langen et al., 1989; Muller et al., 1994a) and in large unilamellar vesicles (Straume & Litman, 1987a). Finally, we note that changing the headgroup from PC to PG in the pair DOPC/DOPG extends the mean lifetime $\langle\tau_F\rangle$.

Table 2: Effect of Lipid Structure on the Time-Resolved Fluorescence Anisotropy of DPH Embedded in Small Unilamellar Vesicles

(A) Analyzed Using the Brownian Rotational Diffusion Model[a]

lipid	χ^2_{red}	β_ν (deg)	λ_2	λ_4	$D_\perp$ (/ns)	$\langle P_2\rangle_{BF}$	$\langle P_4\rangle_{BF}$
POPC	1.24	23	−0.2	−2.1	0.11	0.15	0.28
DOPC	1.31	27	0.1	−1.3	0.09	0.00	0.15
DLPC	1.45	25	0.1	−1.4	0.13	0.00	0.16
DLLPC	1.10	26	1.2	−2.9	0.14	−0.21	0.26
EGGPG	1.16	20	−0.5	−2.1	0.10	0.26	0.31
DOPG	1.18	27	0.1	−1.5	0.08	0.00	0.17
SQDG	1.57	24	0.5	−2.4	0.23	−0.05	0.26
DGDG	1.21	24	0.3	−2.5	0.13	0.01	0.28

(B) Analyzed Using the Compound Motion Model[b]

lipid	χ^2_{red}	β_ν (deg)	λ_2	λ_4	$D_\perp$ (/ns)	θ_{cone} (deg)	$d_\perp$ (/ns)	$\langle P_2\rangle_{BF}$	$\langle P_4\rangle_{BF}$
POPC	1.10	18	−0.4	−1.6	0.08	22	5	0.14	0.15
DOPC	1.31	21	0.1	−0.88	0.07	26	3	−0.01	0.06
DLPC	1.44	20	0.1	−0.91	0.10	22	6	−0.01	0.07
DLLPC	1.10	19	1.1	−2.4	0.13	22	3	−0.20	0.15
EGGPG	1.13	18	−0.7	−1.6	0.07	16	3	0.26	0.21
DOPG	1.15	24	0.1	−1.2	0.07	17	4	−0.01	0.11
SQDG	1.57	21	0.0	−1.7	0.17	21	7	0.06	0.15
DGDG	1.20	21	0.2	−1.7	0.07	23	3	0.00	0.12

[a] Both the results for the phosphatidylcholine and phosphatidylglycerol lipids are given in the order of increasing unsaturation. The order parameters $\langle P_L\rangle_{BF}$ (L= 2, 4) for the fluorophore with respect to the bilayer are calculated using λ_2 and λ_4. From the variation in the values of χ_{red}, the uncertainties in the fitting parameters are estimated as follows: β_ν, 2°; λ_2, 0.2; λ_4, 5%; $D_\perp$, 20%; and order parameters $\langle P_L\rangle_{BF}$, 0.04. [b] The overall order parameters $\langle P_L\rangle_{BF}$ (L = 2, 4) for the fluorophore with respect to the bilayer are calculated using λ_2, λ_4, and θ_{cone}. From the variation in the values of χ^2_{red}, the uncertainties in the fitting parameters are estimated to be as follows: β_ν, 2°; λ_2, 0.2; λ_4, 5%; $D_\perp$, 20%; θ_{cone}, 10°; $d_\perp$, 40%; and overall order $\langle P_L\rangle_{BF}$ parameters, 0.05. For the motion of the cone, we set $D_\parallel = 5D_\perp$ as discussed in the main text. Although CMM and BRD models have a very different physical content, their respective results are seen to be comparable (see Table 2A). Note the lower values for $\langle P_4\rangle_{BF}$ found with CMM.

In Table 2A and Table 2B, the extracted parameters from time-resolved data are displayed, obtained with either the BRD or the compound motion model, respectively. Keeping in mind the slight differences discussed above, the main conclusions are the same for both models. We will successively discuss the columns of these tables.

The emission dipole angle β_ν (column 3) is found to be ∼20° and higher, which agrees with previous findings for TMA-DPH and DPHPC (Muller et al., 1994a,b). Low values appear for the λ parameters (columns 4 and 5), with $|\lambda_4| > |\lambda_2|$ reflecting the bimodal distribution of DPH in lipid vesicle bilayers to be discussed below. The rotational diffusion parameter $D_\perp$ (column 6) gives a measure for the reorientational dynamics of DPH; this parameter is clearly insensitive to the lipid unsaturation as $D_\perp$ is nearly the same, i.e., typically 0.1/ns, for all samples studied, with the exception of SQDG. Interestingly, in bilayers of that lipid, the reorientation is twice as fast.

The results with the CMM for the internal cone parameters, i.e., θ_{cone} and $d_\perp$, are given in Table 2B (columns 7 and 8).

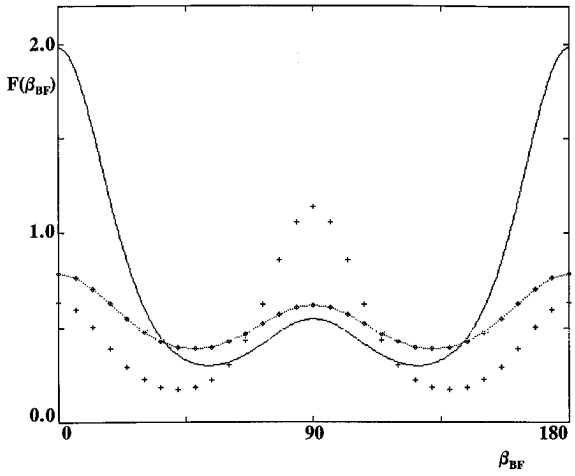

FIGURE 3: Orientational distribution functions $F(\beta_{BF})$ for DPH embedded in small unilamellar vesicle systems of diacylphosphatidylcholine lipids POPC (drawn line), DOPC (string of diamonds) and DLLPC (+ signs). The distribution functions were found using the compound motion model (CMM). β_{BF} is the angle (degrees) of the long molecular axis of the probe with respect to the bilayer normal. The temperature was 20 °C. The population of probe molecules perpendicular to the bilayer normal ($\beta_{BF} = 90°$) is seen to increase with lipid unsaturation.

The cone half-angle θ_{cone} does not vary much with the type of lipid and turns out to have a typical value of 20°. The fast rattling motion is represented by $d_\perp$ and is 2 orders of magnitude faster than the reorientation of the cone itself, as characterized by $D_\perp$. This agrees with the assumptions of the CMM which state that the in-cone motion is uncoupled from and much faster than the motion of the cone itself. We note that these cone parameters can only be extracted with a limited precision as the channel width of 80 ps precludes finer resolution.

Turning to the overall order, the relevant first two order parameters $\langle P_2\rangle_{BF}$ and $\langle P_4\rangle_{BF}$ are given in Table 2A for the BRD model (columns 7 and 8) and in Table 2B (columns 9 and 10) for the CMM. From eq 4, we know that the compound model gives the order parameters as a product of the order parameters for the cone and those for the probe within the cone. Most samples studied here were found to have a positive small value for $r(t{=}\infty)$, i.e., the anisotropy at the long time tail of the decay. From eq 2c, this leaves the sign of $\langle P_2\rangle_{BF}$ undetermined. It is plausible to assume a minus sign for DLLPC vesicles, as Table 2A and Table 2B suggest that the $\langle P_2\rangle_{BF}$ values decrease with unsaturation for the phosphatidylcholine lipids (i.e., POPC has 1, DOPC 2, DLPC 4, and DLLPC 6 double bonds, respectively). Furthermore, the value for $\langle P_2\rangle_{BF}$ is close to zero for DOPC, DLPC, DOPG, SQDG, and DGDG vesicles, while $\langle P_4\rangle_{BF}$ ranges from 0.15 to 0.28. Interestingly, the same values of the order parameters are found for DPH in DOPC and DLPC. In contrast to previous results for TMA-DPH, $\langle P_4\rangle_{BF}$ for DPH turns out to be sensitive to different degrees of unsaturation. We conclude that for DPH, $\langle P_2\rangle_{BF}$ by itself is not a reliable indicator for the order; instead, the full orientational distribution function should be considered. In Figure 3, such distribution functions are given for DPH in PC lipid vesicle bilayers. Corresponding to the small values for the λ parameters, considerable populations of probe molecules lying perpendicular to the bilayer normal are found, especially for DLLPC. Similar transverse populations of DPH have been reported in fully saturated PC vesicles at elevated temperatures by Wang et al. (1991) and in oriented planar DGDG samples by van de Ven et al. (1984). As noted above and exemplified in Figure 1, the CMM fits give reduced transverse populations compared with the BRD fits; this also leads to smaller values for $\langle P_4\rangle_{FB}$ (see Table 2A and Table 2B).

No difference is observed between the order and dynamic parameters of DPH in DOPC and DOPG vesicles. This shows that the differences in chemical composition and even charge of the headgroup have a negligible effect on the inner core of the bilayer. Furthermore, it corresponds well with previous observations that charged fluorescent probes like TMA-DPH do reflect modifications in the lipid headgroup [cf. van Langen et al. (1989) and Muller et al. (1994a)].

We note that the vesicles studied in this paper have diameters larger than 100 nm, i.e., 110 and 185 nm, as determined using dynamic light scattering techniques. However, the population of the extruded DLLPC/DPH systems (diameters around 185 nm) is likely to be in part multilamellar. It has been shown (Hope et al., 1989) that for sufficiently large unilamellar vesicles, i.e., with radii larger than 40 nm, there is no curvature-induced asymmetry between both monolayers. Furthermore, Fenske and Cullis (1993) showed the order parameter profiles in extruded large unilamellar vesicles (LUV) and multilamellar vesicles (MLV) with diameters $\geq$100 nm to be essentially the same.

The present vesicle results can be correlated with previous findings from the literature on three systems: (A) DPH embedded in oriented planar lipid multibilayers; (B) DPH in paraffin oil; and (C) carotenoids in lipid bilayers.

(A) Deinum et al. (1988) performed angle-resolved fluorescence depolarization (AFD) experiments on planar lipid multibilayer samples and used a BRD model for the data analysis. Their results with DPH in POPC, DOPC, DLPC, and DGDG planar multibilayers differ from those for the corresponding vesicles. In the zero-curvature multibilayers, DPH has (1) a much higher order, (2) a significantly reduced $D_\perp$, and (3) a much smaller transverse probe population. This observation can be rationalized in terms of higher water content and bilayer curvature for the vesicle systems and also holds for other probes. EPR experiments on nitroxide spin probes (Korstanje et al., 1989a,b) as well as fluorescence experiments on TMA-DPH (Muller et al., 1994a) led to the same conclusions for these lipid systems. We now find that DPH is more sensitive to bilayer curvature than TMA-DPH as judged by the orientational distributions and the values for $D_\perp$. We conclude that effects of curvature manifest themselves in the core of the bilayer, and not just at the bilayer surface.

(B) Van Langen et al. (1988) studied DPH in paraffin oil where probes have isotropic distribution. On reanalysis of their data using the BRD model we found $D_\perp = 0.07$/ns, close to the value for DOPC SUV in Tables 2, while the order parameters ($\langle P_2\rangle = \langle P_4\rangle = 0.00$) reflected the expected isotropic probe distribution. We note that the value for $\langle P_4\rangle$ differs from our findings for DOPC vesicles while that for $\langle P_2\rangle$ agrees. In conclusion, the dynamics of DPH in paraffin oil and in the hydrocarbon core of DOPC SUV is similar, but the orientational distribution is not. This supports the finding above, that instead of only $\langle P_2\rangle$ we need the entire orientational distribution function to judge the order of DPH.

(C) Apolar polyenes like β-carotene and crocetine share a polyenal backbone with DPH. Johansson et al. (1981) and

van de Ven et al. (1983) concluded that these polyenes orient preferably perpendicular to the surrounding acyl lipid chains in the bilayer. We note that the techniques used by those groups (i.e., linear dichroism and resonance Raman scattering respectively) allow model-independent extraction of order parameters. Apparently, the relative disorder among the lipid acyl chains promotes the transverse orientation in the lipid membrane of even sizable hydrophobic molecules like β-carotene and crocetine. The protecting function of β-carotene as a quencher of oxygen radicals and its role in photochemical energy transfer (Koyama, 1991) might rely on its perpendicular orientation. The fact that both DPH and the structurally related polyenes β-carotene and crocetine tend to orient perpendicularly to the lipid acyl chains in the bilayer suggests that this property is shared by apolar polyene molecules in general.

Comparison of DPH Results with Those Obtained for TMA-DPH and DPHPC in the Same Lipid Bilayer Systems. Collecting results from previous work on TMA-DPH and DPHPC (Muller et al., 1994a,b), the following picture emerges for the behavior of DPH analogues in various lipid bilayer SUV systems. As these analogues reside at different locations in the bilayer, we obtain a depth profile of order and dynamic parameters within the bilayer. TMA-DPH and DPHPC possess a polar headgroup which anchors them at the bilayer−water interface, thus defining their location close to this interface (TMA-DPH) or into the upper part of the acyl chain region (DPHPC); DPH, however, is wholly apolar and unhindered by attached chemical groups, so that it can in principle wander freely within the hydrocarbon core of the bilayer. So a hierarchy for the order parameter $\langle P_2\rangle_{BF}$ in corresponding vesicle systems of PC and PG lipids emerges: TMA-DPH > DPHPC > DPH, i.e., typically 0.4, 0.3, and 0.0 respectively. Typical values for the rotational diffusion parameter are 0.04, 0.02, and 0.1/ns for TMA-DPH, DPHPC, and DPH, respectively. The cone is characterized by values of θ_{cone} around 20° and $d_\perp$ around 3/ns. The latter values are not affected by the choice of the probe. In all cases, we find that the depolarization within the cone proceeds much faster than the reorientation of the cone itself. This is consistent with the assumptions of the CMM.

DOPC Vesicles Containing Gramicidin A. Finally, we discuss our results for DOPC/gA unilamellar vesicles studied with DPH. It is well-known (Killian et al., 1987; Killian, 1992) that gA modulates the lipid phase of emulsions of DOPC in a concentration-dependent way; in such samples, gA can induce an inverted hexagonal H_{II} lipid phase. However, the channel conformation of gA is required to promote this phase transition (Tournois et al., 1987, 1988). Recently, we investigated the effect of gA on vesicle bilayers using the probes TMA-DPH and DPHPC, which scan different regions of the upper part of the bilayer (Muller et al., 1995). Both probes sensed a different effect of the channel and nonchannel peptide conformation on the order and dynamic parameters. This could be explained in terms of the differences in geometrical shape between channel and nonchannel conformations; i.e., the channel and nonchannel conformations are shaped as a diabolo and cylinder, respectively. In this paper, we supplement previous work and employ DPH to probe the perturbation due to gA of the hydrocarbon core of the bilayer.

Here we study the effect of both gA concentration and gA conformation on DOPC SUV. This is done by incorporating the peptide (a) in two conformations and (b) in various peptide:lipid ratios (ranging from 0 up to 10 molar %). The channel or nonchannel conformation of gA was defined by embedding the peptide in the lipid bilayer from TFE and ETOH solution, respectively (Killian, 1992). The results are given in Tables 3 and 4 and in Figures 4 and 5.

Figure 4 shows that the steady-state anisotropy r_{ss} of DPH is sensitive to the conformation of gA, in that channel gA induces a lower r_{ss} than nonchannel gA. This conformational effect correlates well with the main findings of Cox et al. (1992). These authors studied POPC/gA vesicles doped with DPH and measured the steady-state anisotropy of DPH over a concentration range for gA. While both conformations of

Table 3: Effect of Gramicidin A on the Fluorescence Lifetimes of DPH Embedded in Small Unilamellar Lipid Vesicles of DOPC[a]

molar ratio gramicidin A	α_1	τ_1 (ns)	α_2	τ_2 (ns)	$\langle\tau\rangle_F$ (ns)
0%	0.15	3.3	0.85	8.2	7.9
1% nonch	0.34	5.0	0.66	9.2	8.3
1% ch	0.21	2.8	0.79	8.5	8.0
2% nonch	0.17	3.3	0.83	8.7	8.3
10% nonch	0.32	2.0	0.68	8.2	7.6

[a] The molar gramicidin to lipid ratio is given for each sample. Codissolving gA from TFE or ETOH induces the channel (ch) or nonchannel (nonch) conformation, respectively; for each sample, this conformation is indicated. The estimated uncertainties are 5% for α_1, τ_1, α_2, τ_2, and $\langle\tau_F\rangle$. The temperature was 20 °C. The mean fluorescence lifetime $\langle\tau_F\rangle$ is only slightly affected by the presence of gA in either conformation.

Table 4: Effect of Gramicidin A on the Time-Resolved Fluorescence Anisotropy of DPH Embedded in DOPC SUV

(A) Analyzed Using the Brownian Rotational Diffusion Model[a]

gramicidin A molar ratio	χ^2_{red}	β_ν (deg)	λ_2	λ_4	$D_\perp$ (/ns)	$\langle P_2\rangle_{BF}$	$\langle P_4\rangle_{BF}$
0%	1.31	27	0.1	−1.3	0.09	0.00	0.15
1% nonch	2.60	20	−0.3	−1.7	0.09	0.17	0.24
1% ch	1.82	21	0.3	−2.2	0.09	0.00	0.25
2% nonch	1.61	18	0.0	−2.0	0.09	0.24	0.29
10% nonch	1.77	17	0.0	−2.3	0.11	0.14	0.30

(B) Analyzed Using the Compound Motion Model[b]

gramicidin A molar ratio	χ^2_{red}	β_ν (deg)	λ_2	λ_4	$D_\perp$ (/ns)	θ_{cone} (deg)	$d_\perp$ (/ns)	$\langle P_2\rangle_{BF}$	$\langle P_4\rangle_{BF}$
0%	1.31	21	0.1	−0.88	0.07	26	3	−0.01	0.06
1% nonch	1.99	19	−0.4	−1.2	0.06	21	1	0.14	0.13
1% ch	1.81	16	0.2	−2.0	0.08	20	3	0.00	0.17
2% nonch	1.55	18	−0.9	−0.85	0.05	26	2	0.23	0.09
10% nonch	1.81	*	−0.3	−2.1	0.08	*	*	0.18	0.27

[a] Gramicidin A was added to the lipid prior to vesicle preparation. The peptide to lipid molar ratio is indicated as a percentage. Codissolving gA from TFE or ETOH induces the channel (ch) or nonchannel (nonch) conformation, respectively, as indicated for each sample. From the variation in the values of χ^2_{red}, the uncertainties in the fitting parameters are estimated as follows: β_ν, 2°; λ_2, 0.3; λ_4, 5%; $D\perp$, 20%; and order parameters $\langle P_L\rangle_{BF}$, 0.05. It is seen that gA affects the orientational distribution function, while leaving $D_\perp$ unchanged. [b] Codissolving gA from TFE or ETOH induces the channel or nonchannel conformation, respectively; for each sample, this conformation is indicated, as well as the molar peptide concentration. The overall order parameters $\langle P_L\rangle_{BF}$ ($L = 2, 4$) for the fluorophore with respect to the bilayer are calculated using λ_2, λ_4, and θ_{cone}. As discussed in the text, we have set $D_\parallel = 5D_\perp$. From the variation in the values of χ^2_{red}, the uncertainties in the fitting parameters are estimated to be as follows: β_ν, 2°; λ_2, 0.3; λ_4, 5%; $D_\perp$, 20%; θ_{cone}, 10°; $d_\perp$, 40%; and overall order $\langle P_L\rangle_{BF}$ parameters, 0.05. An asterisk denotes an unresolved parameter due to low time resolution as discussed in the main text. Compare with Table 4A and note the similarity of the results obtained with the CMM and BRD models, respectively.

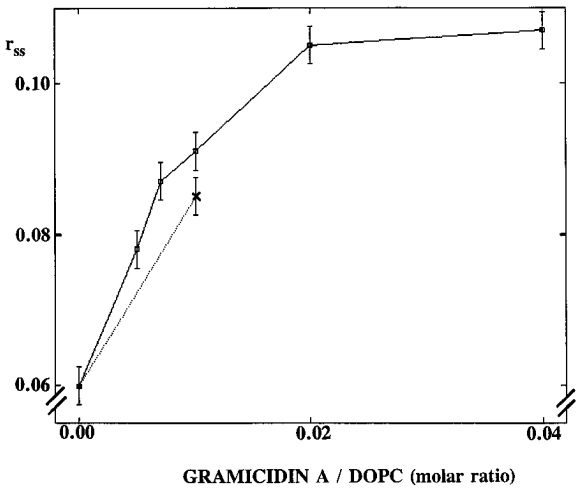

FIGURE 4: Effect of gA concentration and conformation on the steady-state fluorescence anisotropy r_{ss} of DPH in DOPC vesicle bilayers. Results are shown for the channel (lower curve) and nonchannel (upper curve) conformations, which were induced by codissolving gA from TFE or ETOH, respectively. It is seen that initially r_{ss} increases with increasing gA concentration, but saturates at 2 molar % in the nonchannel conformation. Furthermore, at a gA concentration of 1%, the nonchannel conformation has a stronger effect than the channel conformation on the steady-state anisotropy.

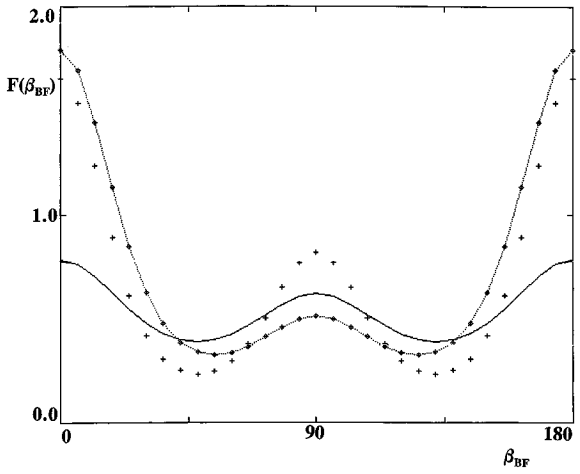

FIGURE 5: Effect of gA concentration and conformation on the orientational distribution function $F(\beta_{BF})$ for DPH reconstructed using the compound motion model. β_{BF} is the angle (degrees) of the long molecular axis of the probe with respect to the bilayer normal. Distribution functions are shown for 0 molar % gA (solid line), 1 molar % channel gA (crosses), and 1 molar % nonchannel gA (string of diamonds). It is seen that nonchannel gA enhances the order better than channel gA.

gA raised r_{ss}, Cox et al. found that the nonchannel conformation was a more effective ordering agent than the channel conformation.

The results from the time-resolved fluorescence lifetime and anisotropy measurements are summarized in Tables 3, 4A, and 4B. Table 3 indicates that the mean lifetime $\langle\tau_F\rangle$ is only slightly affected by the presence of gA; it is generally longer than those of both TMA-DPH and DPHPC. In Table 4A,B, results for the analysis of the anisotropy data are given; the BRD and CMM models were used in the analysis, and both allowed good fits to the data. In Table 4B, the time resolution of 80 ps/channel was insufficient for one sample (indicated by asterisks) to resolve the effects of the emission dipole angle β_ν and the cone half-angle θ_{cone} which both determine the drop of the initial anisotropy (Muller et al., 1994a). However, as the slow motion of the cone is independent of the fast motion within the cone, the slow parameters remain well determined. gA seems only to influence the order parameters strongly, and not the cone diffusion coefficient $D_\perp$; its value remains typically around 0.06/ns. This contrasts with the strong decrease in $D_\perp$ found for DPHPC with increasing concentration of gA (Muller et al., 1995).

The last two columns in Table 4A,B display the order parameters. We find that nonchannel gA increases the order of DPH in DOPC vesicles, at the same time reducing the perpendicular populations at modest concentrations of gA (<10 molar %). However, at low concentrations, channel gA has less effect than nonchannel gA on the distribution function, as seen in Figure 5. This effect of the peptide conformation fully agrees with previous observations on DOPC vesicles using the probe DPHPC. In the core of the DOPC bilayer monitored by DPH and at the intermediate depth probed by DPHPC, the nonchannel conformation orders the lipids, while the channel conformation does not affect the low value for $\langle P_2\rangle_{BF}$. As before, this can be rationalized in terms of the geometrical shape of gA. The cylindrical shape of the nonchannel conformation constrains adjacent fluorophores to a larger extent than the waist of the diabolo formed by the channel conformation.

Conclusions. We have shown that DPH has low values for the second order parameter $\langle P_2\rangle_{BF}$ in various vesicle systems. However, this finding should not be interpreted as implying low molecular order. Inspection of the complete orientational distribution functions shows maxima at 0° and 90°. We find a clear decrease in $\langle P_2\rangle_{BF}$ if the unsaturation is enhanced: this order parameter approaches zero and may even attain negative values. Therefore, $\langle P_2\rangle_{BF}$ on its own should not be taken as a measure of molecular order. For DPH, a substantial fraction of the probe molecules is oriented perpendicular to the membrane bilayer director. Such perpendicular populations are clearly reflected in $\langle P_4\rangle_{BF}$. Its values exceed those of $\langle P_2\rangle_{BF}$. However, we feel that visual inspection of the orientational distribution function for the probe in the bilayer gives the clearest idea of the orientational order. The type of lipid headgroup does not significantly affect the shape of the distribution function. This was expected as DPH resides deep in the hydrocarbon region of the bilayer.

We find that the steady-state anisotropy r_{ss} of DPH in lipid SUV is small. Time-resolved experiments were required to disentangle the effects of the order and the dynamics on the fluorescence anisotropy of DPH in vesicles. It is found that both the CMM and BRD models give comparable results. In particular, both predict a sizable population of probes oriented perpendicular to the bilayer. For DPH, the introduction of an extra degree of motional freedom in the CMM seems not essential for interpretation of the experimental data. In this respect, DPH differs from its polar analogues TMA-DPH and DPHPC. Combining our data for all three probes gives a consistent depth profile of order and dynamic parameters through the lipid bilayer.

Although the BRD and CMM models give equivalent fits to the time-resolved anisotropy decays of DPH, we have shown that these models give different predictions for the correlation functions underlying the anisotropy decay. This implies that experiments which are both time- and angle-resolved should be able to discern between the models.

DPH proved sensitive to the concentration and conformation of the peptide antibiotic gA in DOPC SUV. Our data show that the nonchannel conformation of gA is more effective than the channel form as a promotor of molecular order in the deep acyl chain region of the bilayer. This finding correlates fully with the previous data for the polar probes TMA-DPH and DPHPC. It shows that the two conformations of gA can be distinguished according to their effect on the order parameter profile through the bilayer. This can be rationalized in terms of the geometrical shape of the gA dimer in either the channel or the nonchannel conformation.

ACKNOWLEDGMENT

We thank Drs. J. A. Killian and H. Tournois [Center for Biomembranes and Lipid Enzymology (CBLE), Utrecht University] for the generous gift of HPLC-purified gramicidin A, Dr. H. van Langen for help in collecting the time-resolved anisotropy datasets, Mrs. M. L. de Jong-Verheijden for carrying out the phosphorus, galactose, and sulfate determinations, Mrs. N. S. Postma, M. Sc., and Dr. H. Talsma (Department of Clinical Pharmacology, Utrecht University) for access to and help with the dynamic light scattering apparatus, and Prof. Dr. Y. K. Levine for discussions. The SRS was made available by NWO through the agreement between SERC (Scientific and Engineering Research Council) and NWO. We have benefitted greatly from Dr. D. Shaw's help and discussions at Daresbury Laboratory (U.K.).

REFERENCES

Andersen, O. S., Sawyer, D. B., & Koeppe, R. E., II (1992) in *Biomembrane Structure and Function* (Gaber, B. P., & Easwaran, K. R. K., Eds.) pp 227−244, Academic Press, Schenectady, NY.

Berde, C. B., Andersen, H. C., & Hudson, B. S. (1980) *Biochemistry 19*, 4279−4293.

Best, L., John, E., & Jaehnig, F. (1987) *Eur. Biophys. J. 15*, 87−102.

Cevc, G., & Marsh, D. (1987) *Phospholipid Bilayers. Physical Principles and Models*, J. Wiley & Sons, New York.

Chen, P. S., Toribara, T. Y., & Warner, H. (1956) *Anal. Chem. 28*, 1756−1760.

Cundall, R. B., & Dale, R. E., Eds. (1983) *Time-Resolved Fluorescence Spectroscopy in Biochemistry and Biology*, Plenum Press, New York.

Cox, K. J., Ho, C., Lombardi, J. V., & Stubbs, C. D. (1992) *Biochemistry 31*, 1112−1118.

Davenport, L., Dale, R. E., Bisby, R. H., & Cundall, R. B. (1985) *Biochemistry 24*, 4097−4108.

Deinum, G., van Langen, H., van Ginkel, G., & Levine, Y. K. (1988) *Biochemistry 27*, 852−860.

Dubois, M., Gilles, K. A., Hamilton, J. K., Rebers, P. A., & Smith, F. (1956) *Anal. Chem. 28*, 350−355.

Fenske, D. B., & Cullis, P. R. (1993) *Biophys. J. 64*, 1482−1491.

Heřman, P., Konopásek, I., Plášek, J., & Svobodova, J. (1994) *Biochim. Biophys. Acta 1190*, 1−8.

Hope, M. J., Redelmeier, T. E., Wong, K. F., Rodrigueza, W., & Cullis, P. R. (1989) *Biochemistry 28*, 4181−4187.

Houslay, M. D., & Stanley, K. K. (1983) *Dynamics of Biological Membranes*, J. Wiley & Sons, New York.

Itoh, T., & Kohler, B. E. (1987) *J. Phys. Chem. 91*, 1760−1764.

Johansson, L. B.-A., Lindblom, G., Wieslander, A., & Arvidson, G. (1981) *FEBS Lett. 128*, 97−99.

Killian, J. A. (1992) *Biochim. Biophys. Acta 1113*, 391−425.

Killian, J. A., & Urry, D. W. (1988) *Biochemistry 27*, 7295−7301.

Killian, J. A., Burger, K. N. J., & de Kruijff, B. (1987) *Biochim. Biophys. Acta 897*, 269−284.

Koole, P., Dammers, A. J., van Ginkel, G., & Levine, Y. K. (1984) *Biochim. Biophys. Acta 777*, 297−305.

Korstanje, L. J., van Faassen, E. E., & Levine, Y. K. (1989a) *Biochim. Biophys. Acta 980*, 225−233.

Korstanje, L. J., van Faassen, E. E., & Levine, Y. K. (1989b) *Biochim. Biophys. Acta 982*, 196−204.

Kotyk, A., Janášek, K., & Koryta, J. (1988) *Biophysical Chemistry of Membrane Functions*, Wiley, New York.

Koyama, Y. J. (1991) *Photochem. Photobiol. B*, 265−280.

Lakowicz, J. R. (1986) *Principles of Fluorescence Spectroscopy*, Plenum Press, New York.

Mayer, L. D., Hope, M. J., & Cullis, P. R. (1986) *Biochim. Biophys. Acta 1070*, 209−214.

Mulders, F., van Langen, H., van Ginkel, G., & Levine, Y. K. (1986) *Biochim. Biophys. Acta 859*, 209−218.

Muller, J. M., van Faassen, E. E., & van Ginkel, G. (1994a) *Chem. Phys. 185*, 393−404.

Muller, J. M., van Faassen, E. E., & van Ginkel, G. (1994b) *Biochem. Biophys. Res. Commun. 201*, 709−715.

Muller, J. M., van Ginkel, G., & van Faassen, E. E. (1995) *Biochemistry 34*, 3092−3101.

Ruf, H., Georgalis, Y., & Grell, E. (1989) *Methods Enzymol. 172*, 364−390.

Seelig, A., & Seelig, J. (1977) *Biochemistry 16*, 45−50.

Seelig, A., & Waespe-Sarcevic, N. (1978) *Biochemistry 17*, 3310−3315.

Spencer, B. (1960) *Biochem. J. 75*, 435−440.

Straume, M., & Litman, B. J. (1987a) *Biochemistry 26*, 5113−5120.

Straume, M., & Litman, B. J. (1987b) *Biochemistry 26*, 5121−5126.

Stubbs, C. D., Kouyama, T., Kinosita, K., & Ikegami, A. (1981) *Biochemistry 20*, 4257−4262.

Tournois, H., Killian, J. A., Urry, D. W., Bokking, O. R., de Gier, J., & de Kruijff, B. (1987) *Biochim. Biophys. Acta 905*, 222−226.

Tournois, H., Henseleit, U., de Gier, J., de Kruijff, B., & Haest, C. W. M. (1988) *Biochim. Biophys. Acta 946*, 173−177.

van de Ven, M. J. M., & Levine, Y. K. (1984) *Biochim. Biophys. Acta 777*, 283−296.

van der Heide, U. A., van Zandvoort, M. A. M. J., van Faassen, E. E., & Levine, Y. K. (1993) *J. Fluor. 3*, 269−277.

van der Sijs, D. A., van Faassen, E. E., & Levine, Y. K. (1993) *Chem. Phys. Lett. 216*, 559−565.

van Echteld, C. J. A., de Kruijff, B., Verkleij, A. J., Leunissen-Bijvelt, J., & de Gier, J. (1982) *Biochim. Biophys. Acta 692*, 126−138.

van Gurp, M., van Langen, H., van Ginkel, G., & Levine, Y. K. (1988) in *Polarized spectroscopy of ordered systems* (Samori', B., & Thulstrup, E. W., Eds.) pp 455−490, Kluwer, Dordrecht, The Netherlands.

van Gurp, M., van Heijnsbergen, T., van Ginkel, G., & Levine, Y. K. (1989) *J. Chem. Phys. 90*, 4103−4111.

van Langen, H., Engelen, D., van Ginkel, G., & Levine, Y. K. (1987a) *Chem. Phys. Lett. 138*, 99−104.

van Langen, H., Levine, Y. K., Ameloot, M., & Pottel, H. (1987b) *Chem. Phys. Lett 140*, 394−400.

van Langen, H., van Ginkel, G., & Levine, Y. K. (1988) *Liq. Crystals 3*, 1301−1317.

van Langen, H., van Ginkel, G., Shaw, D., & Levine, Y. K. (1989) *Eur. Biophys. J. 17*, 37−48.

Vogt, T. C. B., Killian, J. A., Demel, R. A., & de Kruijff, B. (1991) *Biochim. Biophys. Acta 1069*, 525−537.

Wallace, B. A. (1990) *Annu. Rev. Biophys. Biophys. Chem. 19*, 127−157.

Wang, S., Beechem, J. M., Gratton, E., & Glaser, M. (1991) *Biochemistry 30*, 5565−5572.

Webb, M. S., & Green, B. R. (1991) *Biochim. Biophys. Acta 1060*, 133−158.

Yeagle, Ph. (1987) *The Membranes of Cells*, Academic Press, New York.

Zannoni, C., Arcioni, A., & Cavatorta, P. (1983) *Chem. Phys. Lipids 32*, 179−250.

BI951409H